JOURNAL OF GUIDANCE, CONTROL, AND DYNAMICS
Vol. 26, No. 3, May–June 2003

Longitudinal Flying Qualities Prediction for Nonlinear Aircraft

Shiyang Ryu*
Samsung Electronics Company, Ltd., Kyungki-Do 442-742, Republic of Korea
and
Dominick Andrisani†
Purdue University, West Lafayette, Indiana 47907

An analysis tool is presented that predicts longitudinal flying qualities of a piloted aircraft subject to elevator rate limiting and nonlinear stick gradient. The method produces an explicit mathematical pilot model for the pitch attitude tracking task. By performing pilot-in-the-loop simulation, flying qualities metrics are computed for evaluation of the level of flying qualities. The proposed method is validated using the flight experiment called HAVE LIMITS flown at the U.S. Air Force Test Pilot School. Good agreement was obtained between our analytical flying qualities prediction and Cooper–Harper pilot ratings obtained in-flight for elevator rate limits of 10–157 deg/s.

Introduction

FLYING qualities (FQ) requirements play a key role in designing flight control systems for piloted aircraft. For highly augmented fly-by-wire-equipped aircraft, the inherent nonlinear elements such as actuator rate or position limiting, hysteresis, and nonlinear stick gradients are known to contribute to aircraft flying qualities. In particular, actuator rate limiting is noteworthy because of the potential for highly unexpected and explosive pilot-induced oscillations (PIOs).[1] Unfortunately, most traditional flying qualities criteria cannot handle these nonlinear effects explicitly. Therefore, a new prediction method that incorporates actuator rate limiting with pilot-in-the-loop flying qualities evaluations needs to be developed.

Prompted by a series of aircraft accidents involving control surface rate limiting, for example, the F-22 and Gripen, the U.S. Air Force embarked on a multiyear program to investigate the causes of PIOs, to develop methods to predict when PIOs are likely to occur and to determine the flying qualities of PIO-prone aircraft.[2–6]

This paper uses the results of the HAVE LIMITS flight-test program conducted in 1997 to investigate the effects of rate limiting. The same aircraft model and nonlinearities (elevator actuator rate limits and nonlinear stick gradients) are considered in our analysis, and the HAVE LIMITS in-flight determined flying qualities (Cooper–Harper pilot ratings and pilot comments) are used to "calibrate" our analytical flying qualities metrics.

Our approach to flying qualities prediction is based on explicit pilot modeling and pilot-in-the-loop analysis. It was hypothesized that if the simulated pilot–vehicle closed-loop system behaves in such a way as to be qualitatively similar to in-flight tracking test time histories, then key measures that affect flying qualities assessment could be deduced from the simulation study. Functionally, the pilot element can be divided into two components. One is a simple linear compensator designed for a linearized aircraft model (without considering nonlinearities), and the other augments this linear compensator when its control signal reaches the point where linearity breaks down. For the latter component, the dynamic antireset windup (DARW) scheme[7] is employed. Originally, the DARW scheme was developed for controller modifications that account for input constraint in the form of rate or magnitude limits. In this work, this DARW scheme is introduced for describing and modeling of the human pilot's adaptive control activity in the presence of nonlinearities.

Our method is similar to that of Bailey and Bidlack[4] in that both depend on time-domain analysis. The approaches differ in the form of the pilot model, the rules for pilot adaptation, the nature of the pitch attitude tracking task, and the method of flying qualities prediction.

The organization of this paper is as follows. First, a brief description of HAVE LIMITS flight experiment is given. Second, with the nonlinear elements of the aircraft ignored, a linear pilot model is proposed to represent the human pilot. A specific rule is developed for pilot modeling with the intention of producing comparable pitch tracking time histories with the flight data at least in the linear regime. Third, the chosen pilot model is augmented to characterize the nonlinear behavior of the human pilot using the aforementioned DARW scheme. Fourth, the pitch attitude tracking task is simulated to compute time-domain measures, which are closely correlated with two significant flying qualities factors, pitch tracking performance and pilot workload. Finally, the flying qualities are predicted by mapping these measures into the flying qualities metric plane, which will be presented later. Note that this method can be extended to incorporate an aircraft compensator to improve flying qualities.[8]

HAVE LIMITS Flight Experiment

The HAVE LIMITS flight experiment is described in Refs. 9 and 10. Flight tests were conducted at the U.S. Air Force Test Pilot School in spring 1997. The NT-33A aircraft was flown to collect in-flight data such as tracking task time histories, pilot comments, and Cooper–Harper and PIO ratings.

Longitudinal Aircraft Model

Three different configurations were evaluated to identify the effect of rate-limiting on different dynamic characteristics. The NT-33A programmable flight control systems enabled the aircraft to assume different pitch attitude dynamic configurations, denoted 2D, 2P, and 2DU. A schematic block diagram is shown in Fig. 1.

The basic configuration 2D was considered to have good short-period flying qualities with its high bandwidth ($\omega_n = 4.9$ rad/s and $\zeta = 0.7$). Configuration 2D was modified by adding a filter, $4/(s+4)$, to the forward path to create configuration 2P. This configuration was expected to be less resistant to rate limiting because of its slow filter. For configuration 2DU, an artificially unstable aircraft was first designed. This unstable system was stabilized with feedback of angle-of-attack α and pitch rate q using variable stability system. In the absence of rate limiting, configuration 2DU would exhibit good short-period characteristics similar to configuration 2D. However, when the rate limit was reached the resulting system had a divergent short-period mode. Figure 1 shows that in the case of configuration 2DU, rate limiting of the actuator implies a breaking down of the feedback path. Table 1 shows a lower-order-equivalent

Received 30 August 2001; revision received 12 March 2002; accepted for publication 3 December 2002.

*Senior Engineer, Digital Media Research and Development Center, Suwon City.
†Associate Professor, School of Aeronautics and Astronautics. Senior Member AIAA.

Table 1 Short period mode characteristics

Configuration	$\theta/\delta_e(s)$	Flying qualities level
2D	$\dfrac{-102.37(s+1.2)e^{-0.116s}}{s^2+2(0.756)(4.8)s+4.8^2}$	1
2P	$\dfrac{4}{s+4}\cdot\dfrac{-102.37(s+1.2)e^{-0.126s}}{s^2+2(0.756)(4.8)s+4.8^2}$	2
2DU	$\dfrac{-119.84(s+1.2)e^{-0.116s}}{s^2+2(0.67)(4.8)s+4.8^2}$	1

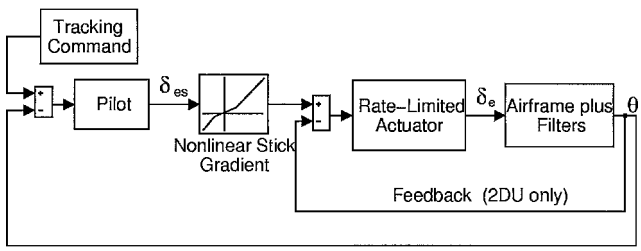

Fig. 1 Longitudinal schematic block diagram of NT-33A model.

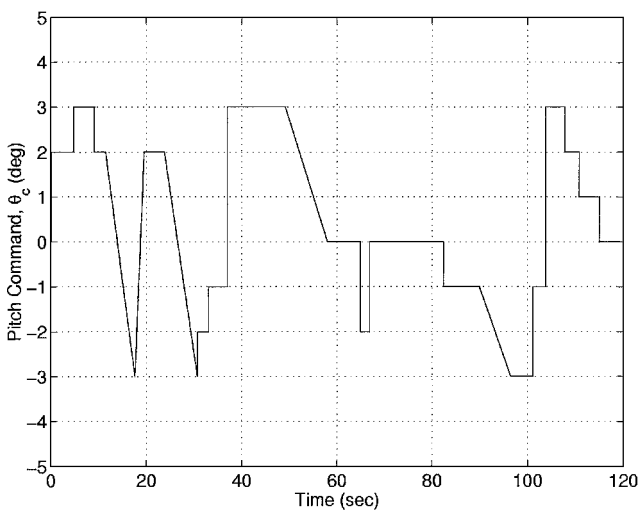

Fig. 2 Discrete pitch tracking task.

system model of each configuration and predicted level of flying qualities with no rate limiting before the flight test.

Tracking Task

Two head-up display (HUD) tracking tasks, discrete task and sum-of-sines task, were adopted to evaluate handling qualities. All configurations were subject to rate limiting on the elevator actuator. The elevator rate limits were 10, 20, 30, 40, and 50 deg/s with a default value of 157 deg/s. At least two of three pilots evaluated each condition. In this study, only the discrete tracking task is used, and the pitch command θ_c time history is provided in Fig. 2.

Results of HAVE LIMITS Flight Test

Figure 3 is a graphical representation of mean Cooper–Harper pilot ratings for discrete task evaluated in flight. Configuration 2D was evaluated as level 1 with no PIO tendency for rate limits of 20 deg/s and above. At an elevator rate limit of 10 deg/s, it was evaluated as level 2 and exhibited PIO tendency. Configuration 2P was evaluated as level 2 for rate limits of 20 deg/s and above. The detrimental effect of the added phase lag caused by smaller rate limits was confirmed. For configuration 2DU, Cooper–Harper ratings ranged from level 1 to uncontrollable, depending on the rate limit. When the rate limit was 157 deg/s, configuration 2DU was evaluated as level 1. However, when the rate limit was decreased below 60 deg/s, it became suddenly divergent as soon as the pilots engaged in aggressive tracking.

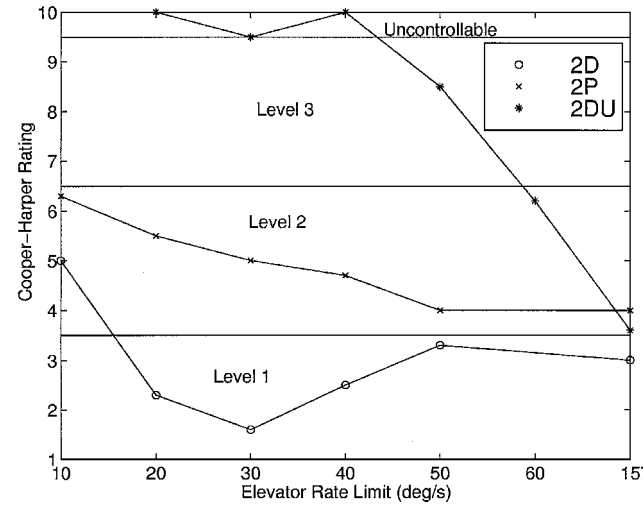

Fig. 3 Cooper–Harper ratings for the HAVE LIMITS flight test.

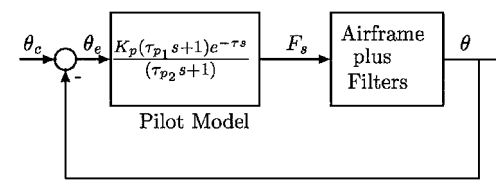

Fig. 4 Conceptual block diagram of pitch attitude tracking.

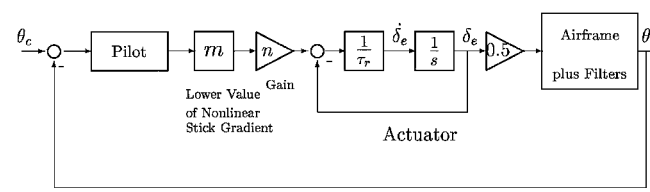

Fig. 5 Pilot-linearized vehicle closed-loop system.

Pilot Modeling for Linear Aircraft Model

In the present work, we use the same structure of pilot transfer function as used in the Neal–Smith criterion.[11] Figure 4 shows a simplified block diagram of its pilot–vehicle closed-loop system. To check if the Neal–Smith pilot modeling standards are applicable to our analysis, pilot model parameters were calculated for the nominal system (configuration 2D). By nominal we mean that the nonlinear stick gradient is linearized about lower gain and rate saturation nonlinearity is ignored (Fig. 5).

Given the values of parameters shown in Fig. 5, $\tau_r = 0.01$, $m = 2.5$, and $n = (2)(2.5)/1.06$, the following Neal–Smith pilot model was obtained with $\omega_{bw} = 3$ rad/s:

$$K_p\frac{(\tau_{p1}s+1)}{(\tau_{p2}s+1)}e^{-\tau s} = 0.237\frac{(0.327s+1)}{(0.339s+1)}e^{-0.3s} \qquad (1)$$

A pilot-in-the-loop simulation was performed using the pitch tracking task with this pilot model, and its result is shown in Fig. 6 with HAVE LIMITS in-flight measured time history data. Note that the pure time delay term, $e^{-0.3s}$, was replaced by a second-order Padé approximation for this simulation. There is considerable mismatch between flight data (Fig. 6a) and simulation data (Fig. 6b). The Neal–Smith pilot modeling rules that were developed from an earlier in-flight experiment[11] seem to be inappropriate for application to the HAVE LIMITS test program. Because we intended the pilot-in-the-loop simulation to be qualitatively similar to the flight data, the pilot model should adequately represent the human pilot's actions when carrying out the task. As a consequence, new pilot modeling rules need to be proposed for our study while maintaining the basic structure of Neal–Smith pilot model transfer function.

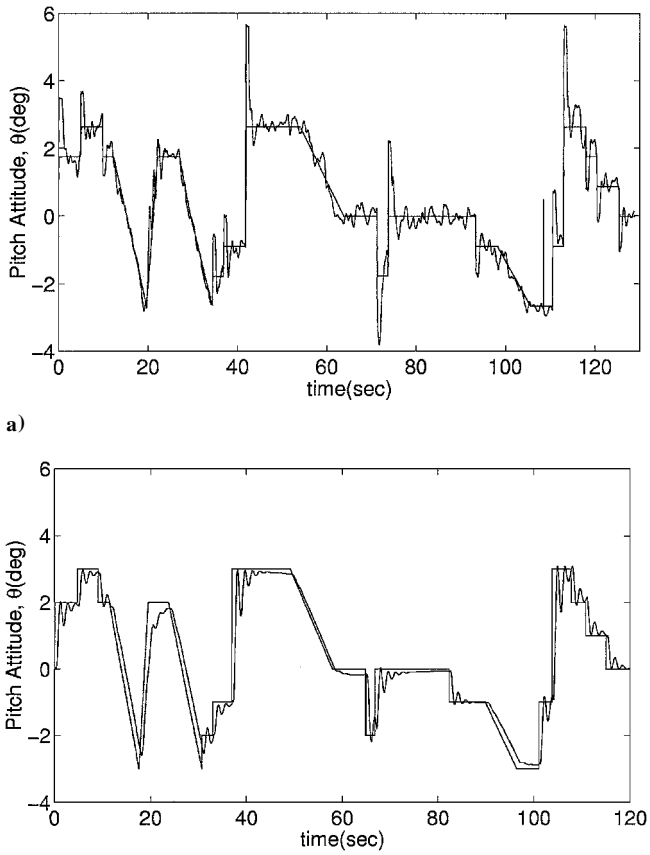

Fig. 6 Comparison of a) flight data and b) simulation result using Neal–Smith pilot model (configuration 2D).

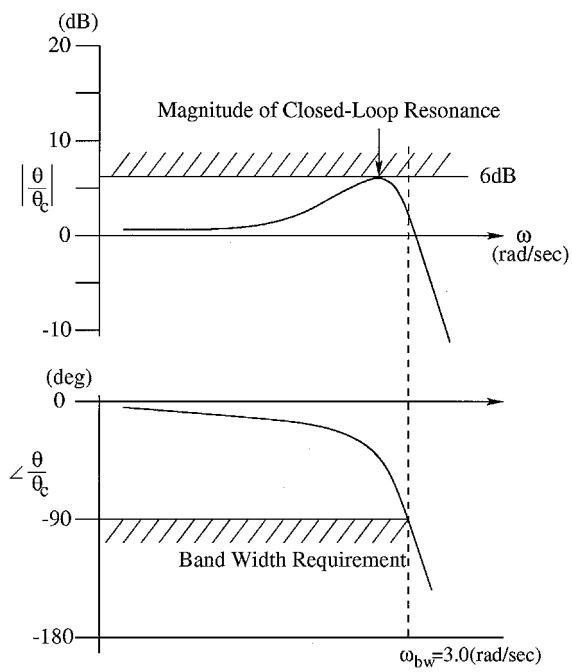

Fig. 7 Modified pilot modeling standards.

On closer examination of the HAVE LIMITS flight data, the following features were observed from the time-domain standpoint.

1) In-flight records (Fig. 6a) show quicker rise time than simulated data of Fig. 6b.

2) Simulated data do not resemble actual flight records due to lack of sizable overshoot (about 80%).

For better qualitative agreement with the in-flight measured time history, pilot modeling rules are modified as follows.

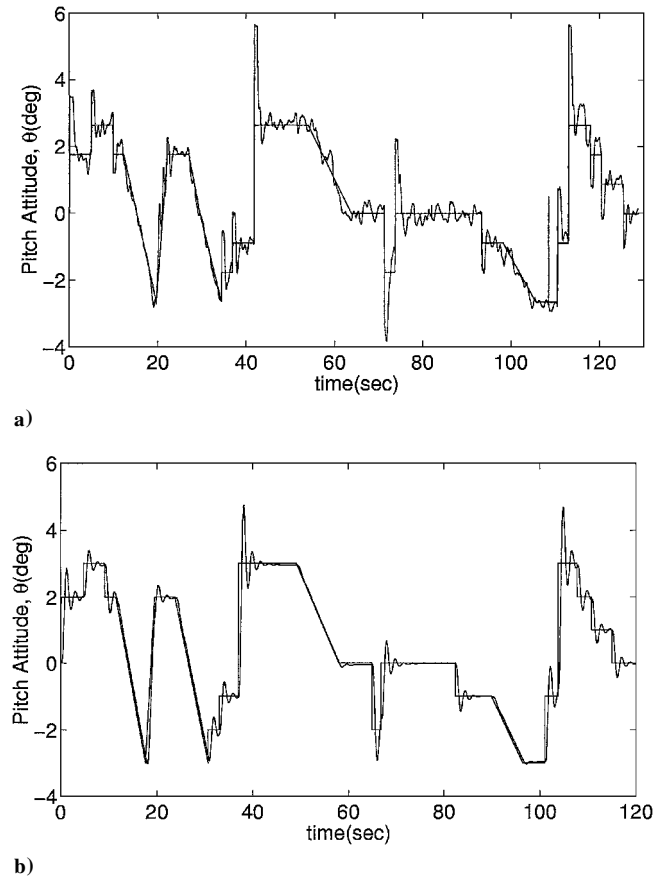

Fig. 8 Comparison of a) flight data and b) simulation result using modified Neal–Smith Pilot Model (configuration 2D).

1) Pilot's time delay τ is decreased from 0.3 to 0.1 for faster response.

2) The magnitude of the closed-loop resonance should be equal to 6 dB for sizable overshoot

3) Bandwidth constraint $\omega_{bw} = 3.0$ rad/s is not altered.

Figure 7 summarizes the rules in terms of a bode plot of the pilot–vehicle closed-loop system. Pitch attitude responses from the HAVE LIMITS data and the simulation using the new pilot model are shown in Fig. 8. The mismatch observed in Fig. 6 was improved considerably. Simple comparison of the flight record (Fig. 8a) and the simulation result (Fig. 8b) may not be pertinent because we used a linearized aircraft model for simulation, whereas the actual flight system 2D includes nonlinear dynamics. However, considering that the rate limit is sufficiently high (157 deg/s) and, under these circumstances, the pilot does not have to move the stick excessively, we can assume the effect of nonlinear behavior in the flight record is negligible. This helps ensure the validity of the modified pilot modeling rules. We will now assume that the pilot model transfer function computed according to these rules can be used for analysis of a high rate-limited flight system.

Nonlinear Pilot Modeling

Although the linear pilot model discussed earlier generated acceptable time responses for a case that was essentially linear, the pilot's adaptations in the presence of nonlinearities cannot be addressed with this simple structure. For a nonlinear pilot modeling formulation, the DARW method[7] is employed. The main advantage of this scheme for our study is that it provides an analytic solution that is simple and unique.

The concept of windup or reset windup was first addressed in proportional integral or proportional integral derivative control systems with input saturation nonlinearities. An interpretation of windup is that the states of the controller do not correspond to the control signal being injected into the plant.[12] The windup problems have been widely observed, and many researchers has provided effective and useful design tools.[13–17]

The DARW scheme involves designing a dynamic compensator based on the following two-step design procedure. First, a linear controller is designed to yield a desirable closed-loop performance ignoring control input nonlinearities. The second step is to augment the existing controller with a compensator to alleviate the adverse effects of any input nonlinearities. We assumed that there is an analogy between the function of this compensator for antiwindup and the pilot's control strategy to minimize performance degradation when the piloted vehicles are subject to nonlinear behavior.

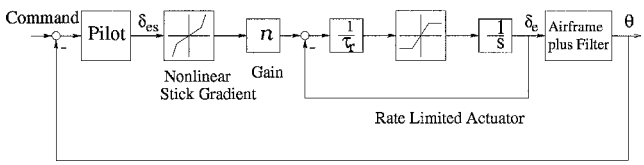

Fig. 9 Nonlinear pilot–vehicle closed-loop system (configurations 2D and 2P).

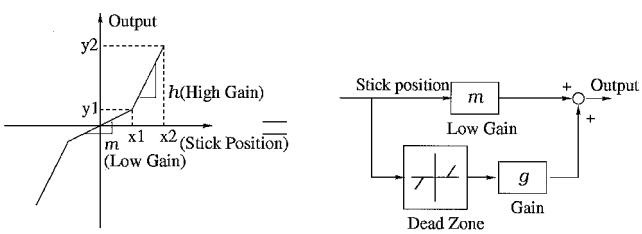

Fig. 10 Two equivalent representations of nonlinear stick gradient.

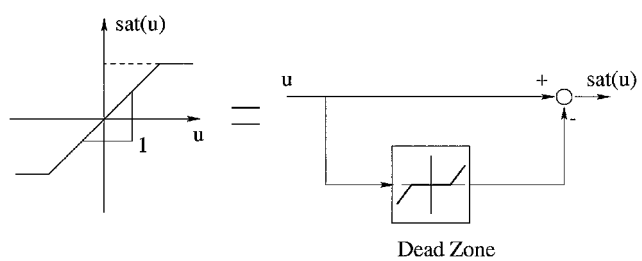

Fig. 11 Two equivalent representations of saturation nonlinearity.

The pilot–vehicle nonlinear system is shown in Fig. 9. For the DARW scheme to be used for this system, the two nonlinear elements are alternatively represented as follows. Figure 10 shows that nonlinear stick gradient can be alternatively expressed via proper combination of gains and dead-zone (DZ) nonlinearity. Note that the value of g can be easily calculated from known parameters shown in Fig. 10a. The saturation nonlinearity is represented in Fig. 11 using the relation $\text{sat}(u) = u - \text{DZ}(u)$, where $\text{sat}(\cdot)$ and $\text{DZ}(\cdot)$ are saturation and DZ nonlinear operators, respectively.

When all nonlinear components are pulled out and lumped together into a single block, the block diagram of Fig. 9 can be redrawn as a system composed of a plant $[P(s)]$, a controller $[K(s)]$, and a diagonal nonlinear operator block Δ as shown in Fig. 12. Note that, in the Fig. 12, Δ_i denote DZ nonlinearities.

The dynamic compensators $[M(s)]$ for configurations 2D and 2P can be obtained from the following equations.

The dynamics of $P(s)$ (from Fig. 12) are

$$\dot{x}_p(t) = A_p x_p(t) + Bu(t), \qquad y(t) = \begin{bmatrix} \theta(t) \\ \delta_e(t) \end{bmatrix} = Cx_p(t)$$

$$u(t) = (mn/\tau_r)v_s(t) + (gn/\tau_r)\hat{v}_s(t) + (1/\tau_r)v_{\delta_e}(t) - \hat{\omega}(t) \quad (2)$$

where $\hat{x} = \text{DZ}(x)$ and the DZ is the nonlinear operator shown in Figs. 10 and 11.

When the notations

$$a = mn/\tau_r, \qquad B_a = B \cdot a, \qquad b = gn/\tau_r$$

$$B_b = B \cdot b, \qquad B_t = B(1/\tau_r)$$

are used, Eq. (2) becomes

$$\dot{x}_p(t) = A_p x_p(t) + B_a v_s(t) + B_b \hat{v}_s(t) + B_t v_{\delta_e}(t) - B\hat{\omega}(t)$$

$$y(t) = Cx_p(t) \quad (3)$$

The dynamics of $K(s)$ (from Fig. 12) are

$$\dot{x}_k(t) = A_k x_k(t) + B_k e(t) \quad (4)$$

$$V(t) = \begin{bmatrix} v_s(t) \\ v_{\delta_e}(t) \end{bmatrix} = C_k x_k(t) + D_k e(t)$$

$$= \begin{bmatrix} C_{k,s} \\ C_{k,\delta_e} \end{bmatrix} x_k(t) + \begin{bmatrix} D_{k,s} \\ D_{k,\delta_e} \end{bmatrix} e(t) \quad (5)$$

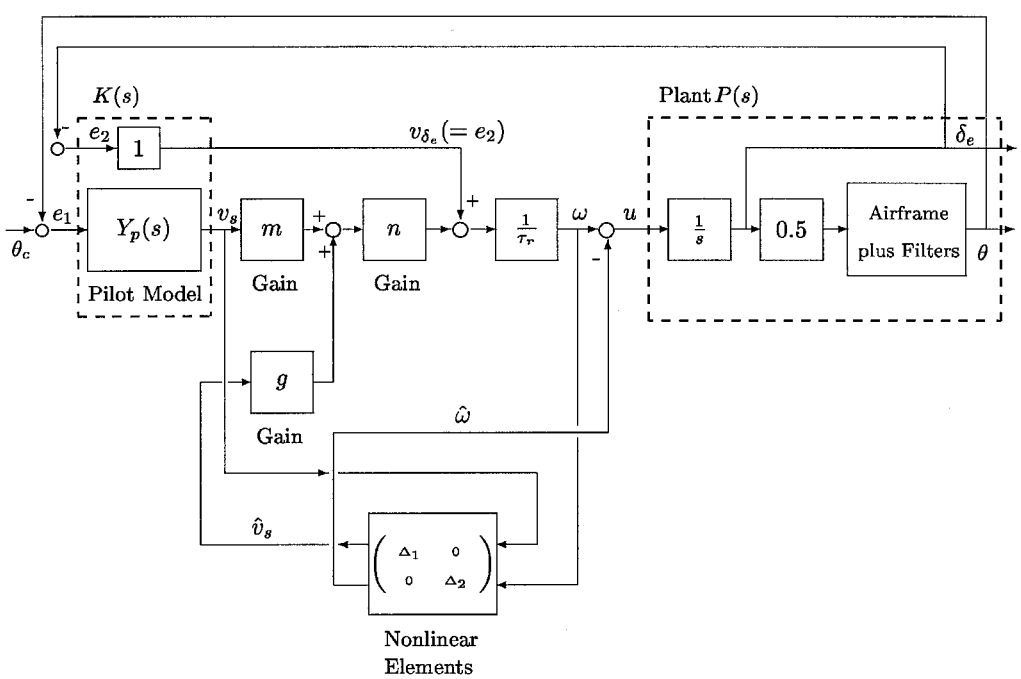

Fig. 12 Pilot-in-the-loop block diagram without pilot compensation for nonlinearities (configurations 2D and 2P).

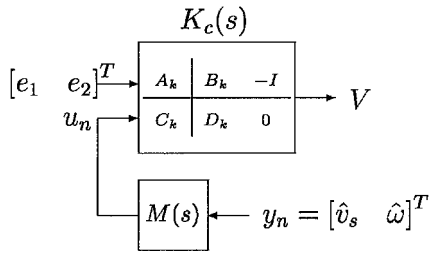

Fig. 13 Nominal controller compensated by $M(s)$.

$$e(t) = \begin{bmatrix} e_1(t) \\ e_2(t) \end{bmatrix} = r(t) - y(t) = \begin{bmatrix} \theta_c(t) \\ 0 \end{bmatrix} - \begin{bmatrix} \theta(t) \\ \delta_e(t) \end{bmatrix} \tag{6}$$

Included in A_k, B_k, C_k, and D_k is the state-space form of the linear pilot model, given in Eq. (1), with the time-delay term represented by a second-order Padé approximation. For application of the DARW scheme, the linear compensator $K(s)$ in Fig. 12 is modified by adding a new input. This is illustrated in the block diagram of Fig. 13, which shows that $K(s)$ is modified to $K_c(s)$ with one more input channel, u_n, from a dynamic antiwindup compensator $M(s)$. This new input captures the action required to adjust the pilot's adaptation to the nonlinear stick gradient and elevator rate limiting. Now $K_c(s)$ can be written as follows. The dynamics of $K_c(s)$ are

$$\dot{x}_k(t) = A_k x_k(t) + B_k e(t) - u_n(t), \qquad V(t) = C_k x_k(t) + D_k e(t)$$
$$e(t) = r(t) - y(t) \tag{7}$$

The dynamic compensator is defined as follows. The dynamics of $M(s)$ are

$$\dot{x}_m(t) = A_m x_m(t) + B_m y_n(t), \qquad u_n(t) = C_m x_m(t) + D_m y_n(t)$$
$$y_n(t) = \begin{bmatrix} \hat{v}_s(t) \\ \hat{\omega}(t) \end{bmatrix} \tag{8}$$

We have established the equations of standard setup for the DARW scheme. The basic idea of the DARW scheme is to make the states of the saturated controller (linear pilot model in our case) as close to the states of the unsaturated controller as possible. Let $x_k(t)$ and $\bar{x}_k(t)$ be the controller states in the absence of and in the presence of input saturation, respectively. The performance index can be described as follows:

$$\min_{M(s)} J = \int_0^\infty \|x_k(t) - \bar{x}_k(t)\|^2 \, dt \tag{9}$$

where $\|\cdot\|$ is the Euclidean norm.

To find an optimal solution for $M(s)$ in Eq. (9), the closed-loop system can be rewritten separately, depending on the absence or the presence of nonlinearities.

1) The dynamics of the closed-loop system in the absence of nonlinearities is as follows: From Eqs. (3–6) and $\hat{v}_s = \hat{\omega} = 0$,

$$\begin{bmatrix} \dot{x}_k(t) \\ \dot{x}_p(t) \end{bmatrix} = A_L \begin{bmatrix} x_k(t) \\ x_p(t) \end{bmatrix} + \begin{bmatrix} B_k r(t) \\ B_L D_k r(t) \end{bmatrix} \tag{10}$$

where

$$A_L := \begin{bmatrix} P & Q \\ R & S \end{bmatrix} := \begin{bmatrix} A_k & -B_k C \\ B_L C_k & A_p - B_L D_k C \end{bmatrix} \tag{11}$$

$$B_L = [B_a \quad B_t] \tag{12}$$

2) The dynamics of the closed-loop system in the presence of nonlinearities is as follows: From Eqs. (3), (7), and (8)

$$\begin{bmatrix} \dot{\bar{x}}_k(t) \\ \dot{\bar{x}}_m(t) \\ \dot{\bar{x}}_p(t) \end{bmatrix} = A_N \begin{bmatrix} \bar{x}_k(t) \\ \bar{x}_m(t) \\ \bar{x}_p(t) \end{bmatrix} + \begin{bmatrix} B_k r(t) - D_m \hat{N}(t) \\ B_m \hat{N}(t) \\ B_L D_k r(t) + B_N \hat{N}(t) \end{bmatrix} \tag{13}$$

where

$$A_N = \begin{bmatrix} A_k & -C_m & -B_k C \\ 0 & A_m & 0 \\ B_L C_k & 0 & A_p - B_L D_k C \end{bmatrix} \tag{14}$$

$$\hat{N}(= y_n) = \begin{bmatrix} \hat{v}_s \\ \hat{\omega} \end{bmatrix}, \qquad B_N = [B_b \quad -B] \tag{15}$$

where the overbar indicates that the corresponding state variables are involved with nonlinearities.

Let $M(t)$ be an impulse response matrix from y_n to u_n in Eq. (8), that is,

$$M(t) := \mathcal{L}^{-1}\{M(s)\} = \mathcal{L}^{-1}\left\{D_m + C_m(sI - A_m)^{-1}B_m\right\} \tag{16}$$

where $\mathcal{L}$ is Laplacian operator. Then, one obtains the following equation from Eq. (7):

$$\dot{x}_k(t) = A_k x_k(t) + B_k e(t) - M(t) * \hat{N}(t) \tag{17}$$

where the asterisk denotes the convolution operator.

By Parseval's theorem, the performance index J can be rewritten as

$$J = \frac{1}{2\pi j} \int_{-j\infty}^{j\infty} \|x_k(s) - \bar{x}_k(s)\|^2 \, ds \tag{18}$$

where the relation, $\mathcal{L}[x(t)] = x(s)$ was used and $s(= \sigma + jw)$ is a complex variable.

From the Laplace transform of Eqs. (10), (13), and (17), one obtains

$$x_k(s) - \bar{x}_k(s) = \Xi_1(s)\hat{N}(s) + \Xi_2(s)r(s) \tag{19}$$

where $\Xi_1(s)$ and $\Xi_2(s)$ are given by

$$\Xi_1(s) = Y(s)^{-1}\left[B_k C(sI - S)^{-1}B_N + M(s)\right] \tag{20}$$

$$\Xi_2(s) = [(sI - P) - Q(sI - S)^{-1}R]^{-1}\left[B_k + Q(sI - S)^{-1}B_L D_k\right]$$
$$- Y(s)^{-1}\left[B_k - B_k C(sI - S)^{-1}B_L D_k\right] \tag{21}$$

$$Y(s) = (sI - A_k) + B_k C\left[(sI - S)^{-1}B_L C_k\right] \tag{22}$$

For $\Xi_1(s)$ to be zero,

$$M^*(s) = -B_k C(sI - S)^{-1}B_N$$
$$= B_k C[sI - (A_p - B_L D_k C)]^{-1}[-B_b \quad B] \tag{23}$$

Note that $\Xi_2(s) = 0$ from the definition of P, Q, R, and S given in Eq. (11).

The dynamic compensator $M^*(s)$ in Eq. (23) is the optimal solution for Eq. (9) and will be used for nonlinear pilot modeling. More detailed mathematical development procedures including nonsingular property of $Y(s)$ in Eqs. (20–22) and stable property of A_L in Eq. (11) are provided in Ref. 18.

Figure 14 illustrates how the dynamic compensation is implemented for a nonlinear aircraft model (configuration 2D or 2P). In the block diagram, for simplicity, the realization of linear pilot model $Y_p(s) = C_y(sI - A_y)^{-1}B_y + D_y$ was used because the feedback loop of δ_e passes through directly without affecting the states

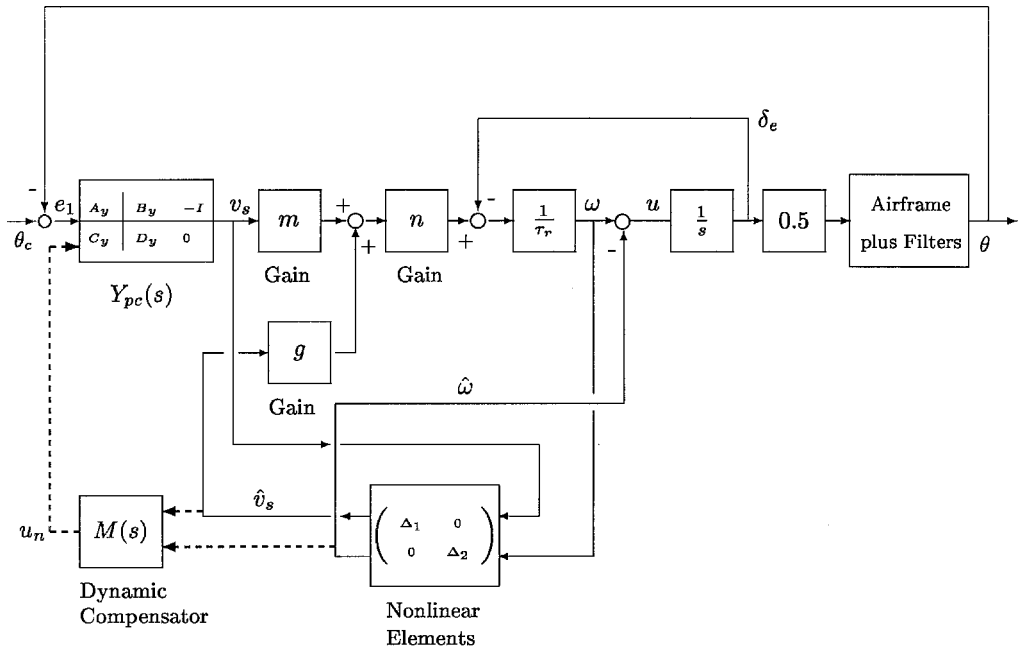

Fig. 14 Pilot-in-the-loop block diagram with pilot compensation for nonlinearities (configurations 2D and 2P).

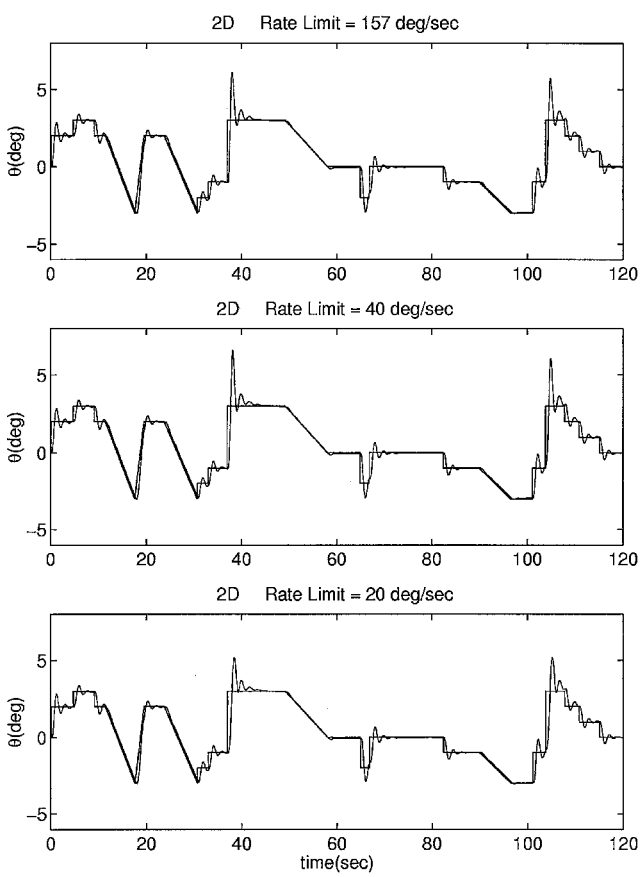

Fig. 15 Pilot-in-the-loop simulation using pilot model of Fig. 14 (configuration 2D).

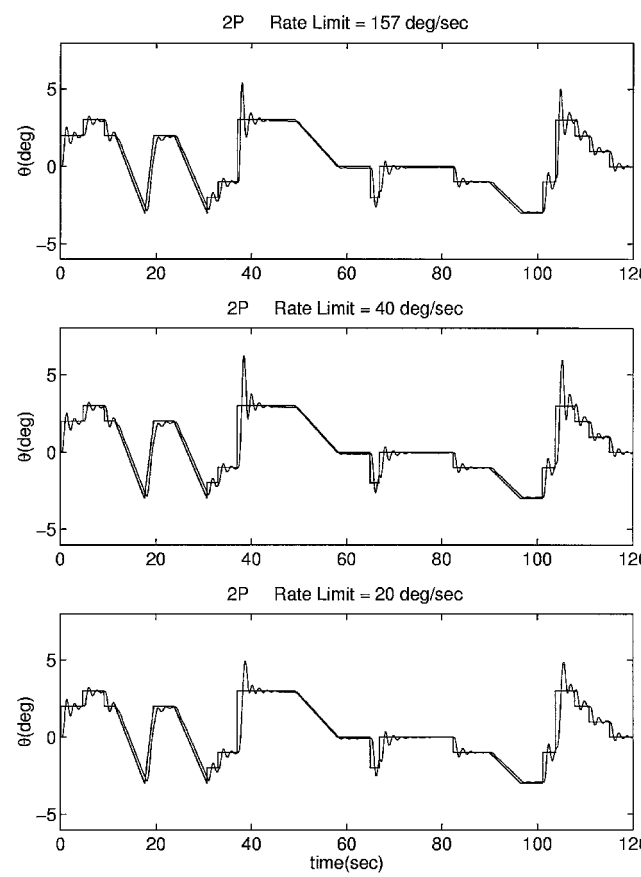

Fig. 16 Pilot-in-the-loop simulation using pilot model of Fig. 14 (configuration 2P).

of $K_c(s)$ shown in Fig. 12. The procedure of finding $M(s)$ for configuration 2DU is similar and omitted for brevity.

Nonlinear Simulation Results

With the nonlinear pilot model just described, a nonlinear simulation of the pitch tracking task was performed for each configuration for different rate limits. The purpose of this simulation was to identify main factors that contribute to flying qualities evaluation.

Flying qualities are not just stability properties, but involve more intricate properties that needs to be quantified in terms of pilot workload and closed-loop performance. This is the reason why we relied on time-domain simulation rather than attempting to develop an analytic method for flying qualities assessment of nonlinear aircraft. The pitch attitude time histories of the nonlinear pilot-in-the-loop simulation are shown in Figs. 15–17. Numerical data used in the simulation are given in Table 2.

Table 2 Parameter values of aircraft model

Parameters	Values
Gain m	2.5
Gain g	6.3636
Gain n	(2.5)(2)/1.06
Actuator time constant τ_r	0.01
Stick position in Fig. 10, x_1	0.9
x_2 (Fig. 10)	3.5
Stick output in Fig. 10, y_1	2.25
y_2 (Fig. 10)	25.29

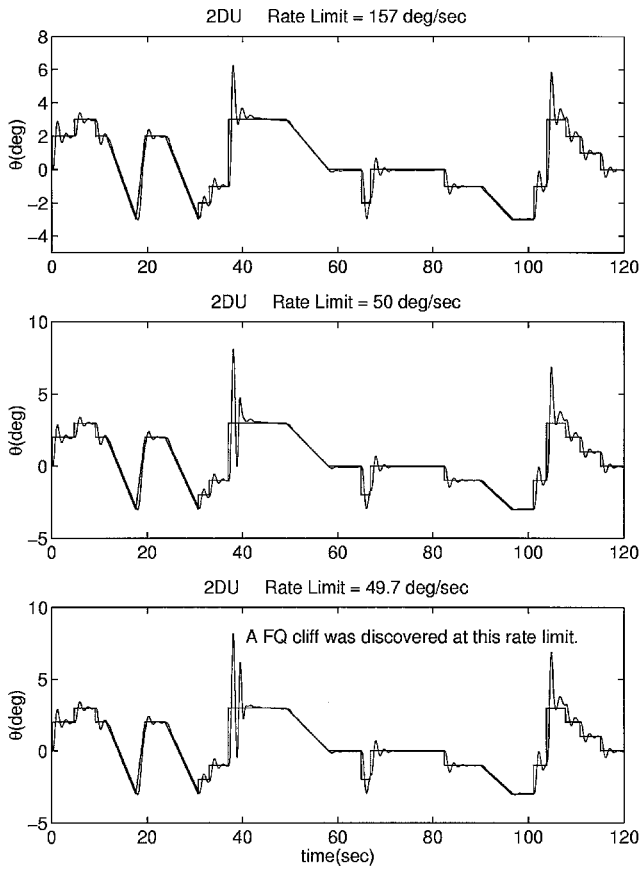

Fig. 17 Pilot-in-the-loop simulation using our proposed pilot model (configuration 2DU).

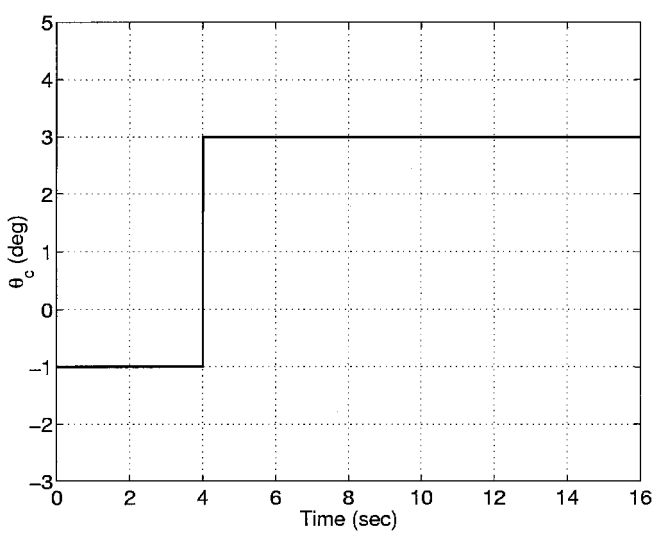

Fig. 18 Simplified tracking task command used for the development of flying qualities metrics.

The resulting closed-loop time responses for both configurations 2D and 2P remained stable under all conditions. However, the simulated time responses of configuration 2DU were stable only for rate limits of 49.7 deg/s and above (Fig. 17). A small further decrease in this rate limit destabilized the simulated closed-loop system and exhibited divergent phenomenon. This agrees with the flying qualities cliff that was discovered near 50 deg/s of elevator rate limit in the HAVE LIMITS flight experiment.

From the simulation study, we noted that the pitch attitude response can be best characterized where an aggressive and large-amplitude step command is imposed, for example, near the 35-s point in Figs. 15–17. Henceforth, instead of the whole 120-s simulation (Fig. 2), a simplified 16-s tracking command (Fig. 18) was used for the development of flying qualities prediction metrics.

HAVE LIMITS flight data and our simulation time responses are overplotted and compared to each other in Figs. 19 and 20. Qualitative agreement is quite apparent between the piloted flight data and the nonlinear analytical pilot-in-the-loop simulation data.

Development of Flying Qualities Metrics

Flying qualities are often defined by two primary factors, closed-loop performance and pilot workload.[19] Our basic rules in determining flying qualities metrics are that they must be expressed directly in terms of what the pilot would see or feel in tracking tasks, and they must effectively capture the important aspects of performance and workload.

In this study, the performance metric is chosen to be the weighted sum of root-mean-square (rms) pitch attitude tracking error and rms value of pitch rate (see Fig. 14),

$$J_p = w_e \left\{ \frac{1}{N} \sum_{i=1}^{N} [\theta_c(t_i) - \theta(t_i)]^2 \right\}^{\frac{1}{2}} + w_q \left\{ \frac{1}{N} \sum_{i=1}^{N} [q(t_i)]^2 \right\}^{\frac{1}{2}} \tag{24}$$

where w_e and w_q are weights suitably chosen for scaling ($w_e = 2$ and $w_q = 1$).

The pilot workload metric consists of the following two additive parts:

$$J_w = w_s \left\{ \frac{1}{N} \sum_{i=1}^{N} [\dot{v}_s(t_i)]^2 \right\}^{\frac{1}{2}} + w_{u_n} \left\{ \frac{1}{N} \sum_{i=1}^{N} [u_n(t_i)]^T u_n(t_i) \right\}^{\frac{1}{2}} \tag{25}$$

where $\dot{v}_s$ is the rate of change of stick position and u_n is the compensation (vector) signal fed back to the pilot model ($w_s = 0.6$ and $w_{u_n} = 2$). The sample time between data points was 0.01 s.

On examination of the simulation, it turned out that the rate-of-change of stick position is a more sensitive indicator as a workload metric than stick position. The second term of J_w addresses pilot effort for sensitive stick operation for fine tracking when actuator rate limiting is encountered. In the actual flight experiment[9] with low rate limits, pilots commented that, during gross acquisition following a big target step, they had to release the stick or back out of the loop to eliminate the winding up of the aircraft. It was hypothesized that the compensation action of $M(s)$ in our closed-loop system is analogous to this human pilot's adaptive control strategy.

With the performance index J_p and workload index J_w defined earlier, the flying qualities metric plane is drawn in Fig. 21 using a format suggested in Refs. 4 and 11. Each aircraft dynamic configuration, 2D, 2P, and 2DU, for the various rate limits, was mapped into the plane by simulating tracking task (Fig. 18) and computing J_p and J_w. The flying qualities level boundaries were drawn on the basis of median pilot ratings obtained from the HAVE LIMITS flight experiment.

As can be seen from Fig. 21, there is a good correlation between in-flight Cooper–Harper pilot ratings and our analytical flying qualities prediction boundaries. The poor dynamic configurations 2D at the rate limit of 10 deg/s and 2P with all rate limits are related to a large workload measure J_w. In fact, the flight data indicate

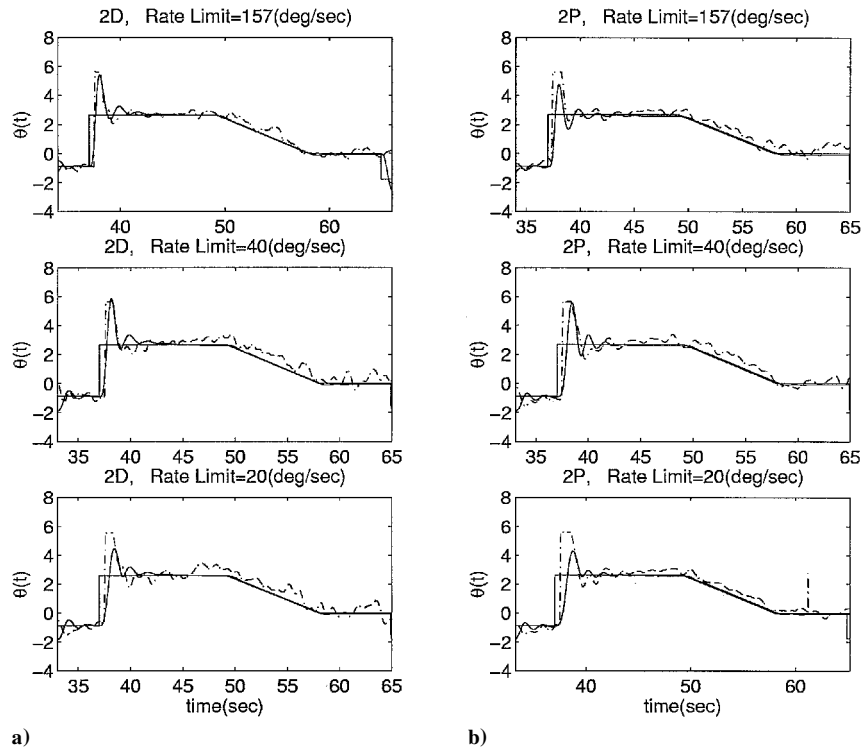

Fig. 19 Comparison of the pilot-in-the-loop simulation using the proposed method with the HAVE LIMITS data for a) configuration 2D and b) configuration 2P: ——, simulation results and –·–, HAVE LIMITS data.

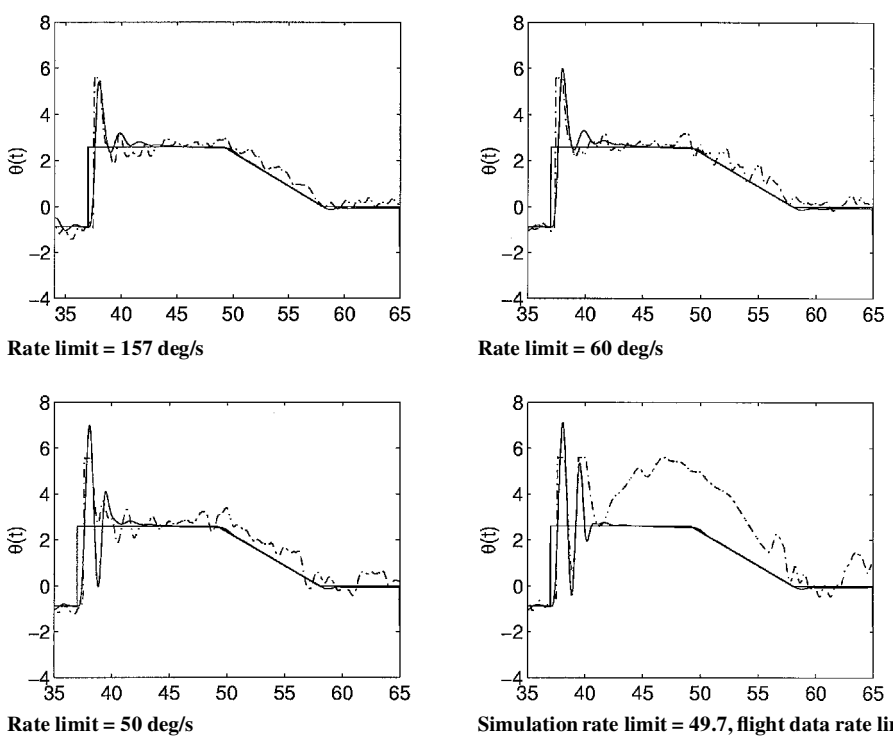

Fig. 20 Comparison of the pilot-in-the-loop simulation using the proposed method with the HAVE LIMITS data for configuration 2DU: ——, simulation results and –·–, HAVE LIMITS data.

that slow response and pilot's intense workload to remain in phase are the main objectionable difficulties for these configurations. The dramatic flying qualities degradation of configuration 2DU can be seen from its large performance measure J_p. This has correlations with large overshoot and abrupt response during the pilot's gross maneuvering for target acquisition in the flight-test data. Overall, a system with good dynamic characteristics (configuration 2D) is less sensitive to the effect of actuator rate limiting. Figure 21 shows that both the performance metric J_p and the workload metric J_w are required to describe correctly the flying qualities observed by the pilots in the HAVE LIMITS experiment. Note that the partial dotted line between level 3 and uncontrollable means that it is undefined for lack of data.

Note that the flying qualities metrics that we developed serve not only as a prediction tool but also as a guideline for the design of an aircraft flight control system that improves flying qualities.[8]

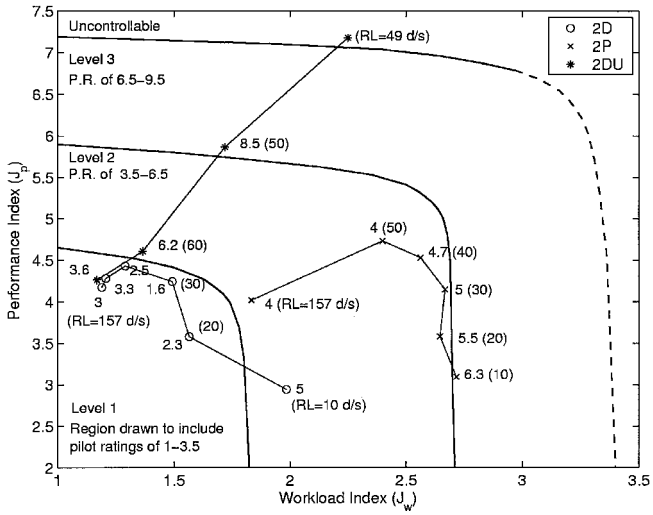

Fig. 21 Flying qualities correlation of simulation-determined flying qualities metrics with HAVE LIMITS flight-determined Cooper–Harper pilot ratings: numbers indicate average Cooper–Harper rating and ( ) enclose rate limits.

Conclusions

An analysis tool to predict longitudinal flying qualities of a piloted nonlinear aircraft subject to elevator rate limiting and nonlinear stick gradient was developed. The analysis tool was validated against to the Cooper–Harper pilot ratings obtained in the HAVE LIMITS flight experiment.

The time-domain approach was employed in an effort to produce simulation responses that are qualitatively similar to the flight data. This approach turned out to be useful in describing the dynamic behavior of nonlinear pilot–vehicle system. In particular, during the development of our analysis tool, nonlinear stick gradient as well as rate limiting was identified to play a significant role in flying qualities for this experiment.

Both a performance metric and a workload metric were required to separate the various configurations into flying qualities level regions.

Good agreement was obtained between flying qualities regions drawn on our computational flying qualities metric plot and the Cooper–Harper pilot ratings obtained in-flight.

References

[1]Klyde, D. H., McRuer, D. T., and Myers, T. T., "Pilot-Induced Oscillation Analysis and Prediction with Actuator Rate Limiting," *Journal of Guidance, Control, and Dynamics*, Vol. 20, No. 1, 1997, pp. 81–89.

[2]Klyde, D. H., McRuer, D. T., and Myers, T. T., "Unified Pilot-Induced Oscillation Theory, Vol. 1: PIO Analysis with Linear and Nonlinear Effective Vehicle Characteristics, Including Rate Limiting," U.S. Air Force Wright Labs., Rept. WL-TR-96-3028, Wright–Patterson AFB, OH, Dec. 1995.

[3]Anderson, M., and Page, A., "Unified Pilot-Induced Oscillation Theory, Vol. 3: PIO Analysis Using Multivariable Methods," U.S. Air Force Wright Labs., Rept. WL-TR-96-3030, Wright–Patterson AFB, OH, Dec. 1995.

[4]Bailey, R. E., and Bidlack, T. J., "Unified Pilot-Induced Oscillation Theory, Vol. 4: Time-Domain Neal-Smith Criterion," U.S. Air Force Wright Labs., WL-TR-96-3031, Wright–Patterson AFB, OH, Dec. 1995.

[5]Foringer, L. A., and Leggett, D. B., "An Analysis of the Time-Domain Neal-Smith Criterion," AIAA Paper 98-4250, Aug. 1998.

[6]Zeyada, Y., Hess, R. A., and Siwakosit, W., "Analysis of Aircraft Handling Qualities and Pilot-Induced Oscillation Tendencies with Actuator Saturation," AIAA Paper 98-4334, Aug. 1998.

[7]Park, J., and Choi, C., "Dynamic Compensation Method for Multivariable Control Systems with Saturating Actuators," *IEEE Transactions on Automatic Control*, Vol. 40, No. 9, 1995, pp. 1635–1640.

[8]Ryu, S., and Andrisani, D., "Controller Design for Longitudinal Flying Qualities Improvement in Nonlinear Aircraft," AIAA Paper 2000-3988, Aug. 2000.

[9]Kish, B. A., "A Limited Flight Test Investigation of Pilot-Induced Oscillation Due to Elevator Rate Limiting," U.S. Air Force Flight Test Center, AFFTC-TR-97-12, Edwards AFB, CA, Aug. 1997.

[10]Mitchell, D. G., Kish, B. A., and Seo, J. S., "A Flight Investigation of Pilot-Induced Oscillation Due to Rate Limiting," *IEEE Aerospace Conference Proceedings*, Vol. 3, IEEE Publications, Piscataway, NJ, 1998, pp. 59–74.

[11]Neal, T. P., and Smith, R. E., "An In-Flight Investigation to Develop Control System Design Criteria for Fighter Airplanes," Cornell Aeronautical Lab., U.S. Air Force Flight Dynamics Labs., Rept. AFFDL-TR-7074, June 1970.

[12]Kothare, M. V., "Control of Systems Subject to Constraints," Ph.D. Dissertation, California Inst. of Technology, Pasadena, CA, 1997.

[13]Doyle, J. C., Smith, R. S., and Enns, D. F., "Control of Plants with Input Saturation Nonlinearities," *Proceedings of American Control Conference*, American Automatic Control Council, Evanston, IL, 1987, pp. 1034–1039.

[14]Åström, K. J., and Wittenmark, B., *Computer Controlled Systems: Theory and Design*, Prentice–Hall, Englewood Cliffs, NJ, 1984.

[15]Hanus, R., Kinnaert, M., and Henrotte, J. L., "Conditioning Technique, a General Anti-windup and Bumpless Transfer Method," *Automatica*, Vol. 23, 1987, pp. 729–739.

[16]Kothare, M. V., Campo, P. J., Morari, M., and Nett, C. N., "A Unified Framework for the Study of Anti-windup Designs," *Automatica*, Vol. 30, 1994, pp. 1869–1883.

[17]Kapoor, N., and Teel, A. R., "A Dynamic Windup Compensation Scheme Applied to a Turbofan Engine," *Proceedings of the 36th Conference on Decision and Control*, Inst. of Electrical and Electronics Engineers, Piscataway, NJ, 1997, pp. 4689–4694.

[18]Ryu, S., "Longitudinal Flying Qualities and Controller Design for Nonlinear Aircraft," Ph.D. Dissertation, Purdue Univ., West Lafayette, IN, 1999.

[19]Harper, R. P., and Cooper, G. E., "Handling Qualities and Pilot Evaluation," *Journal of Guidance, Control, and Dynamics*, Vol. 9, No. 5, 1986, pp. 515–529.